Magnesium Technology 2013
Edited by: Norbert Hort, Suveen N. Mathaudhu, Neale R. Neelameggham, and Martyn Alderman
TMS (The Minerals, Metals & Materials Society), 2013

Magnesium Technology 2013

Wrought Materials II

Magnesium Technology 2013
Edited by: Norbert Hort, Suveen N. Mathaudhu, Neale R. Neelameggham, and Martyn Alderman
TMS (The Minerals, Metals & Materials Society), 2013

RECRYSTALLIZATION BEHAVIOR OF A MgAlCa ALLOY DURING THERMOMECHANICAL PROCESSING AND SUBSEQUENT HEAT TREATMENT

V.M. Miller, T.M. Pollock

Materials Department; University of California, Santa Barbara, CA 93106-5050

Keywords: AXJ810, Texture, Fine Grain, Thixomolding, Thermomechanical Processing, Recrystallization

Abstract

Microstructure refinement via static and dynamic recrystallization during thermomechanical processing is crucial to the development of wrought magnesium product with desirable combinations of strength and ductility. Microstructural evolution in thixomolded AXJ810 is investigated during warm rolling and subsequent annealing at 300°C and 450°C using scanning electron microscopy and electron backscatter diffraction. The rolled sheets exhibited a partially recrystallized microstructure with a strong basal texture. Significant grain refinement was observed during both static and dynamic recrystallization. Retarded grain growth and strong texture randomization were observed only in regions containing intermetallic particles.

Introduction

As the lowest density structural metal, magnesium and its alloys are highly attractive engineering materials for lightweighting. However, Mg alloys tend to have low formability at room temperature, rendering conventional deformation processing unsuitable and hindering widespread implementation. It has been demonstrated that microstructures with a fine grain size and a low degree of preferred crystallographic orientation ("texture"), can produce ductile behavior in magnesium alloys at room temperature [1-3].

Microstructural refinement and changes in texture are often achieved in magnesium alloys through recrystallization during hot deformation and subsequent annealing. One promising approach is for producing these desirable microstructural features is thixomolding and thermomechanical processing (TTMP). Previous research in Mg-Al-Zn alloys has produced TTMP sheet material with yield strengths above 250MPa and elongations above 14% [4-5].

In the present study, the TTMP process is applied to a Mg-Al-Ca-Sr alloy. The additions of calcium and strontium to Mg-Al alloys has been shown to be an effective means to improve creep resistance at a lower cost than rare earth additions [6-8]. Recent work on this class of alloys demonstrates that the alloy studied, AXJ810, is composed of three major phases upon solidification: α-Mg, β-$Mg_{17}Al_{12}$, and the $(Mg, Al)_2Ca$ Laves phase with a dihexagonal C36 structure [9]. At lower temperatures, the C36 phase will transform to the Al_2Ca C15 phase; however, this transformation is kinetically slow [10]. Therefore, the C36/C15 transformation is not examined further in this study.

Experimental

Thixomolded 3mm thick plates of AXJ810, composition shown in Table I, were warm rolled in one pass at an approximate temperature of 250°C to a 50% reduction in thickness. The sheets were then subjected a flattening treatment at 270°C for two minutes. Additional heat treatments of varied duration below the β-solvus at 300°C and above the β-solvus at 450°C. were then conducted.

Table I. Composition (wt%) of AXJ810 alloy

Al	Ca	Sr	Mn	Mg
8.0	1.02	0.31	0.20	bal.

Microstructural characterization was carried out via scanning electron microscopy (SEM), energy dispersive spectroscopy (EDS). Texture and grain size measurements were made using electron backscatter diffraction (EBSD) measurements from a minimum of 10,000 grains. An FEI DB235 microscope equipped with an EDAX Orientation Imaging Microscopy system was used for SEM, EDS, and EBSD measurements. Additional microstructural observation was carried out using an FEI Tecnai T20 transmission electron microscope (TEM). Material was characterized in the as-molded, as-TTMP, and post-TTMP heat treated states. SEM samples were mechanically polished to 1μm diamond paste, then etched for ten seconds in a 1:10 solution of o-phosphoric acid in methanol. Samples for EBSD and TEM were mechanically polished, then ion milled using the Gatan Precision Ion Polishing System. Fraction recrystallized was estimated as the fraction of grains with the grain reference orientation deviation of less than 1°.

Results

As-Molded Microstructure

In the as-molded condition, the AXJ810 microstructure consists of consists of large particles that were not melted during the molding process surrounded by a matrix of equiaxed fine grains, as shown in Figure 1. The grain boundaries are decorated by the intermetallic phases, β-$Mg_{17}Al_{12}$ and the C36 phase. The average grain size, excluding the unmelted particles, is 6.5μm, while the diameter of the unmelted particles ranges from approximately 20μm to greater than 60μm. Significant amounts of porosity are also observed.

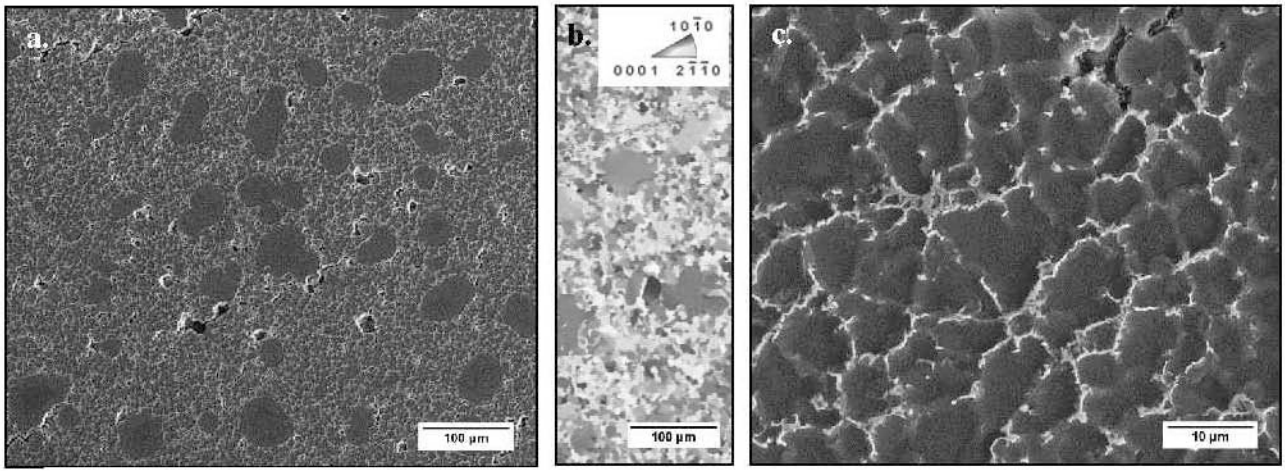

Figure 1. As-molded microstructure in secondary electron imaging (a, c) and an inverse pole figure map (b).

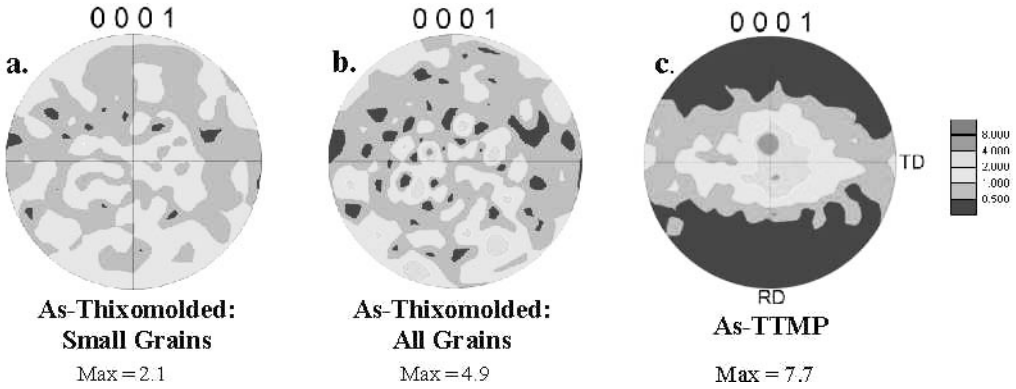

Figure 2. As-molded microstructure in secondary electron imaging (a, c) and an inverse pole figure map (b).

Texture analysis of the as-molded material shows some weak texture due to sampling bias caused by the presence of the large unmelted particles, as shown in Figures 2a and b. Exclusion of these particles reveals a nearly random orientation distribution, with a peak intensity of 2.1 multiples of random distribution (MRD).

As-TTMP Microstructure

After the TTMP process, the microstructure is partially recrystallized, and additional β–$Mg_{17}Al_{12}$ has precipitated, as shown in Figure 3. The average grain size measured via EBSD is 1.5µm. The as-TTMP material also possesses a strong, doubly peaked basal texture, as shown in Figure 4. The measured peak intensity of 7.7 MRD, though this is likely understated due to the sampling bias toward recrystallized grains.

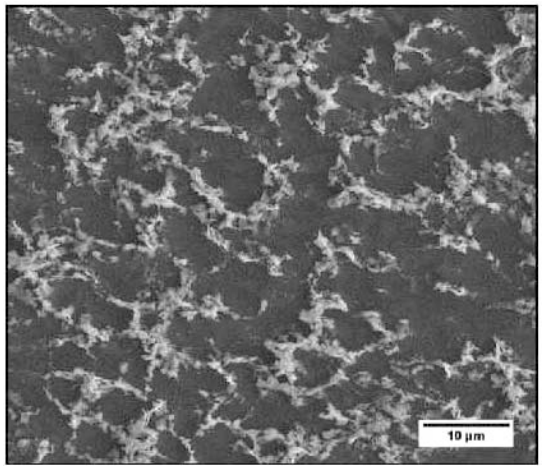

Figure 3. As-TTMP microstructure.

300°C Heat Treatments

Post-TTMP heat treatment at 300°C results in >80% fraction recrystallized within the first five minutes of annealing, and increased to >90% recrystallized after 24 hours. Minimal dissolution of the β phase is observed at short annealing times, though it partially dissolves during the longer heat treatments, as shown in Figure 4. The recrystallized grain size observed after 5 minutes is 4.9µm, and only a slight increase to 5.1µm is observed after 24 hours annealing, as summarized in Table II. The larger grains from unmelted particles are not observed. After recrystallization, a major reduction in texture is observed, with a peak intensity of 3.1 MRD after 5 minutes and 3.3 MRD after 24 hours, as shown in Figure 4a and b.

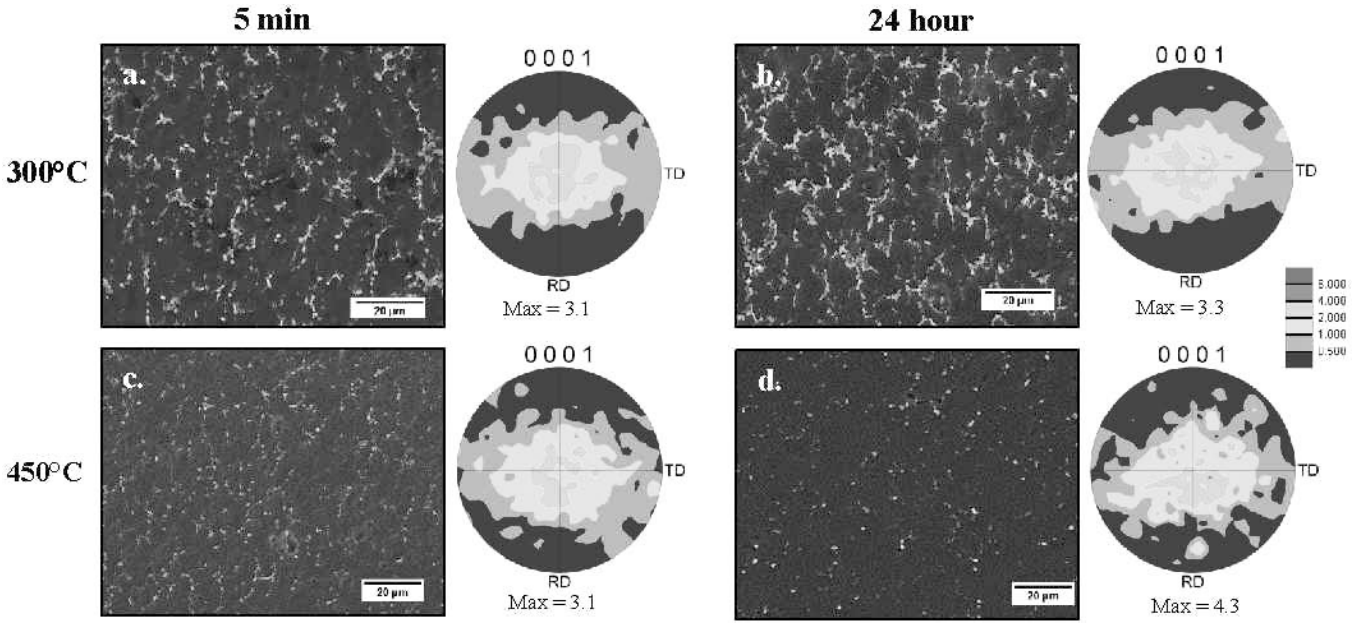

Figure 4. Secondary electron micrographs and EBSD (0001) pole figures for the 5 minute (a, c) and 24 hour (b, d) heat treatments at 300°C (a, b) and 450°C (c, d).

450°C Heat Treatments

Heat treatment at 450°C also produces a >80% recrystallized microstructure within five minutes, with >90% recrystallized after 24 hours, as shown in Figure 4c and d. However, unlike at 300°C, nearly complete dissolution of the β phase was achieved after less than 5 minutes. The recrystallized grain size observed after 5 minutes is 4.6µm, which increases to 7.1µm after 24 hours. The peak texture intensity after 5 minutes is 3.1 MRD, but this increases to 4.3 MRD after 24 hours.

Table II. Average grain diameter (d) after 5 minute and 24 hour heat treatments

Temperature	d after 5 minutes	d after 24 hours
300°C	4.0µm	4.9µm
450°C	4.6µm	7.1µm

Intermetallic-Free Regions

In material subjected to longer heat treatments at both temperatures, regions with a grain size larger than average were observed. Inverse pole figure maps and EDS maps, as shown in Figure 5, were used to confirm that these regions correspond to areas of low alloy content created by the unmelted grains in the original thixomolded material. The Al/Ca overlay EDS map clearly denotes the locations of intermetallic particles. A region free of intermetallics is present in the lower portion of the image, corresponding with the coarse-grained region in the IPF map.

Grain size and texture analysis was conducted independently on the intermetallic-containing and intermetallic-free regions. Note that the sample size for the intermetallic-free regions (approximately 500 grains) was significantly smaller than that of the intermetallic-containing regions due to the lower fraction

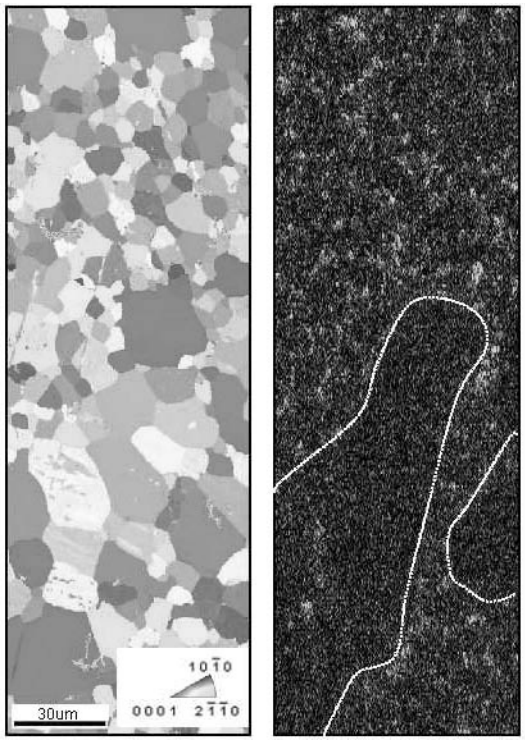

Figure 5. Inverse pole figure map (left) and Al/Ca EDS map (right) of material heat treated at 450°C for 24 hours demonstrating that the coarse-grained region is largely free of intermetallic particles, outlined in white on the EDS map.

present in the material. After 5 minute heat treatments, neither temperature showed any statistically significant difference in grain size in the intermetallic free regions. The average grain size

Table III. Average grain diameter (d) after 24 hour heat treatments

Temperature	d (intermetallic-containing region)	d (intermetallic-free region)
300°C	5.1μm	13.8μm
450°C	7.1μm	15.4μm

after 24 hours at each heat treatment temperatures is presented in Table III.

Basal pole figures, shown in Figure 6, were calculated independently for the intermetallic-containing and intermetallic-free regions of a sample heat treated at 450°C for 24h. These regions were partitioned using a grain size criterion and were visually correlated with EDS maps to ensure accuracy. However, this grain size criterion prevents a similar analysis from being conducted on material subjected to a shorter post-TTMP heat treatment. The pole figure calculated from the intermetallic-containing regions shows a lower value of peak intensity than the un-partitioned data. Additionally, the pole figure representing the intermetallic-containing region shows a more significant spread of the basal poles in the transverse direction.

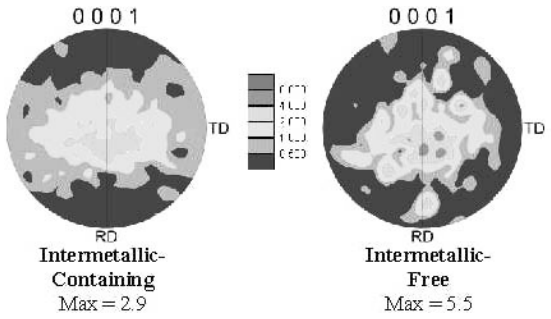

Figure 6. Basal pole figures of the intermetallic-free and intermetallic-containing regions in a sample heat treated at 450° C for 24 hours.

Discussion

At both heat treatment temperatures, recrystallization occurs rapidly and produces a fine grain size with significant degree of texture randomization.

Grain Growth

Severe grain growth was not observed in any of the heat treatment conditions in this study. Particle pinning effects appear to be effective in restricting the grain size, as evidenced by comparison of the regions with and without intermetallic particles. Grain growth appears to be significantly more severe without the presence of intermetallic particles.

Additionally, only small differences in the extent of grain growth was observed between the two heat treatment temperatures, despite the complete dissolution of the β phase at 450°C. The extent of coarsening observed at both temperatures is low in comparison to the extent of grain coarsening in the intermetallic-free regions. The similarity in the extent of grain coarsening regardless of the presence of the β phase indicates that the C36 phase alone is effective at pinning the grain boundaries and stabilizing the small grain size.

Texture Development

Regions containing intermetallic particles show dramatic texture weakening at longer heat treatment times. This is atypical; static recrystallization, particularly without the presence of intermetallic particles generally does not result in major texture weakening [11-12]. Particle stimulated nucleation (PSN) of recrystallization would help to explain the texture weakening in the presence of intermetallic particles. However, considering the low degree of texture observed after the 5 minute heat treatments, additional work is necessary to verify whether the stronger texture observed in the absence of intermetallics is a result of oriented nucleation or oriented growth.

At the shortest heat treatment duration, 5 minutes, the fraction recrystallized and the recrystallization texture appeared to be unaffected by the heat treatment temperature and corresponding β phase fraction. Shorter heat treatment durations are necessary to discern any effects that exist.

Conclusions

In the AXJ810 alloy, the TTMP and subsequent heat treatment process is highly effective for producing material with a low degree of texture and a fine grain size, suggesting it will have good room temperature formability. Comparison of regions with and without intermetallic particles demonstrates that the particles play a critical role in texture randomization and stabilization of the fine grain structure during recrystallization and grain growth. The presence of the thermally-stable C36 phase is effective at restricting grain growth to temperatures above the β solvus, allowing for enhanced microstructural control during heat treatment.

Acknowledgements

The authors would like to thank nanoMAG, LLC for providing the material used in this study.

References

1. J. Koike *et al.*, "The activity of non-basal slip systems and dynamic recovery at room temperature in fine-grained AZ31B magnesium alloys," *Acta Materialia*, 51 (7) (2003), 2055-2065.

2. R. Gehrmann, M. Frommert, and G. Gottstein, "Texture effects on plastic deformation of magnesium," *Materials Science and Engineering: A*, 395, (1-2) (2005), 338-349.

3. M. Barnett, D.L. Atwell, and A. Beer, "Grain Size in Mg Alloys: Recrystallization and Mechanical Consequences," *Materials Science Forum*, 558-559 (2007), 433-440.

4. T.D. Berman *et al.*, "Microstructure Evolution in AZ61 During TTMP and Subsequent Annealing Treatments," *Magnesium Technology*, eds. W. Sillekens *et al.* (Wiley, 2011), 599-603.

5. T.D. Berman *et al.*, "Microstructure Modification and Deformation Behavior of Fine Grained AZ61L Sheet Produced by

Thixomolding and Thermomechanical Processing," *Magnesium Technology 2012*, eds. S.N. Mathaudhu *et al.* (Wiley, 2012), 339-344.

6. M.O. Pekguleryuz and A.A. Kaya, "Creep Resistant Magnesium Alloys for Powertrain Applications," *Advanced Engineering Materials*, 5 (12) (2003), 866-878.

7. A.A. Luo, B.R. Powell, and M.P. Balogh, "Creep and Microstructure of Magnesium-Aluminum-Calcium Based Alloys," *Metallurgical and Materials Transactions A*, 33 (3) (2002), 567-574.

8. K. Hirai *et al.*, "Effects of Ca and Sr addition on mechanical properties of a cast AZ91 magnesium alloy at room and elevated temperature," *Materials Science and Engineering: A*, 403 (1-2) (2005), 276-280.

9. A. Suzuki *et al.*, "Phase equilibria in the Mg-Al-Ca ternary system at 773 and 673K," *Metallurgical and Materials Transactions A*, 37 (12) 2006, 975-983.

10. A. Suzuki *et al.*, "Structure and transition of eutectic (Mg, $Al)_2Ca$ Laves phase in die-cast Mg-Al-Ca base alloy," *Scripta Materialia*, 51 (10) (2004), 1005-1010.

11. X. Yang, H. Miura, and T. Sakai, "Recrystallization Behaviour of Fine-Grained Magnesium Alloy After Hot Deformation," *Transactions of Nonferrous Metals Society of China*, 31 (2007), 1139-1142.

12. R.K. Nadella, I. Samajdar, and G. Gottstein, "Static Recrystallisation and Textural Changes in Warm Rolled Pure Magnesium," *Magnesium: Proceedings of the 6th International Conference on Magnesium Alloys and Their Applications* (2005), 1052-1057.